# Disappearance of nuclear magicity towards drip lines

R. C. Nayak

*Department of Physics, G. M. College, Sambalpur-768004, India*

Using the mass predictions of the recently developed infinite nuclear matter model of atomic nuclei, we show here that the *classical* magic numbers disappear under exotic condition of neutron or proton excess. This localized nature of the magic numbers supports the reported strong quenching of the magic shells implied from the study of astrophysical *r*-process nuclidic abundances, and in agreement with the experimental trends observed in the low-mass region. An important offshoot of the present study is the identification of the characteristic local energies of the model as the carrier of shell structure. [S0556-2813(99)00811-0]

PACS number(s): 21.10.Dr. 21.10.Pc. 21.60.Cs, 26.30.+k

## I. INTRODUCTION

It is well known that the ground-state properties of nuclei lying in the $\beta$-stable valley exhibit characteristic irregularities in the otherwise smooth behavior at specific neutron and/or proton numbers indicating the existence of shell structure as well as the so-called magic numbers in nuclei. In the language of the shell model, such magic-number nuclei have closed-shell structure leading to their pronounced stability. But nuclei being composite bound-systems of interacting neutrons and protons, it is natural to ask the question [1] of whether the observed magicity of the magic numbers of neutrons or protons is localized in nucleon space, and if not, to what extent these are influenced by the number of nucleons of opposite kind present in the system. For $\beta$-stable nuclei, the neutron-to-proton ratio being nearly unity, the answer has been traditionally in the negative. However, with rapid developments taking place in the technology for producing such exotic neutron and proton rich nuclei in recent years, this question has become crucial, and especially so in the light of its implications on various nucleo-astrophysical problems [2]. Conversely a direct answer to this question remains illusive as masses of such exotic nuclei are not yet known. However in the low-mass region where masses are already known, the decreased magicity of the magic neutron numbers 20 and 28 in the neutron-drip ($n$-drip) region has been already shown [3,4]. Complementing this observation, the highly shrinking shell-closure feature has also been reported from a recent astrophysical calculation [2,5,6] of the nuclear abundances of heavy elements, which are mostly believed to have been generated through rapid neutron-capture process ($r$-process) of nucleosynthesis. This has been further corroborated by the Hartree-Fock-Bogoliubov (HFB) calculations with SKP [7] force. Moreover, Chen *et al.* [6] even succeeded in removing the reported anomaly earlier observed in the $r$-process nuclidic abundance curves, using the masses obtained from the spherical HFB calculation [8]. Also, a model study [9] with this Bogoliubov-quenching phenomenologically included in the extended Thomas-Fermi plus Strutinsky integral (ETFSI) model [10], was found to remove the reported anomalies in the abundance curves, which were earlier seen [2,6] using the mass predictions of the ETFSI as well as the finite-range droplet model (FRDM) [11]. But the canonical model [6] which calculates the abundances using the predicted masses, was itself questioned [12]

on the grounds that the model is too simplistic to warrant any significant implication on the nature of shell closure. Nevertheless, the shell-quenching feature being shown as a solution of the $r$-process nuclidic abundances cannot be ignored altogether. Moreover it is a well-established feature in the low mass region.

In view of the crucial role of this question, we report here its answer for the higher magic neutron numbers $N_m = 50$, 82, and 126 from the mass predictions [13] of the recently improved [14] version of the infinite nuclear matter (INM) model [15,16] of atomic nuclei. This model as such has been found to be quite successful not only as a mass model [16,13], but also for the extraction [14] of nuclear saturation properties including the nuclear incompressibility coefficient $K_\infty$, apart from resolving the so-called $r_0$ paradox [17]. In particular we find that the shell gaps at the neutron-magic numbers almost disappear not only towards the neutron-drip ($n$-drip) line, but towards the proton-drip ($p$-drip) line as well. It would not be exaggerating to remark that the shrinking of neutron-magicity towards the $p$-drip line is perhaps demonstrated here for the first time. We get this answer from the systematic behavior of the two-neutron separation energies ($S_{2n}$) calculated from the predicted masses. This is further reinforced in a more decisive manner by the characteristic behavior of the so-called local energies ($\eta$), which are incidentally the key quantities for the INM model to succeed as a mass formula. Moreover, these quantities are determined following a well-defined ensemble-averaging procedure from an ensemble of values generated for each nucleus, by repeated application of the recursion relations involving the $\eta$'s of neighboring nuclei from all possible sides of the nuclear chart. Hence as a byproduct of this study, a well-defined physical basis for the characteristic local energies of the INM model emerges as the carrier of nuclear shell structure.

In Sec. II, we briefly pinpoint the salient features of the INM model to facilitate our discussion about the method of extracting the local energies and the results thereupon. Section III deals with the actual method of the extraction process. In Sec. IV, we present the results concerning the identification of typical closed-shell behavior in the known valley. The results concerning the behavior of magic shell closures in the exotic drip regions are presented in Sec. V. Section V also discusses the possible implications on the role

of spin-orbit potentials in the exotic regions. Finally we present the summary and conclusions in Sec. VI.

## II. BRIEF OUTLINE OF THE INM MODEL

The details of the INM model along with its recent improvements can be found elsewhere [15,16,14,18]. Here we just highlight the basic ingredients of the model to facilitate our later discussion. Fundamentally, the INM model has outgrown from the generalized [19] Hugen Holtz–Van Hove (HVH) [20] theorem of many-body theory, which is perfectly valid for any interacting many-fermion system. For asymmetric nuclear matter, the theorem primarily connects three observable, namely, the neutron and proton Fermi energies $\epsilon_n = (\partial E / \partial N)_Z$, $\epsilon_p = (\partial E / \partial Z)_N$ and the mean energy per particle $E/A$ as

$$E/A = \frac{1}{2}[(1+\beta)\epsilon_n + (1-\beta)\epsilon_p], \quad (2.1)$$

where $\beta$ is the asymmetry parameter $(N-Z)/(N+Z)$. This theorem is exact for nuclear matter and has been shown [20] to be independent of the form of the actual nuclear interaction and remains valid even in the presence of multibody forces [18]. Its extension to finite nuclei is again based on the premise [15,16] that the energy $E^F$ of a finite nucleus can be considered equivalent to the energy $E^S$ of a sphere made up of infinite nuclear matter at the ground-state density plus a residual energy $\eta$, called the local energy:

$$E^F(A,Z) = E^S(A,Z) + \eta(A,Z). \quad (2.2)$$

$E^S$ being the energy of INM sphere is written as

$$E^S(A,Z) = E(A,Z) + f(A,Z), \quad (2.3)$$

where

$$f(A,Z) = a_s^I A^{2/3} + a_c^I \left[ Z^2 - 5\left(\frac{3}{16\pi}\right)^{2/3} Z^{4/3} \right] A^{-1/3} - \delta(A,Z) \quad (2.4)$$

denotes the finite-size effects of the sphere, which are global in nature. $\delta(A,Z)$ is the usual pairing energy term given by

$$\delta(A,Z) = +\Delta A^{-1/2} \quad \text{for even-even nuclei}$$

$$= 0 \quad \text{for odd-}A \text{ nuclei}$$

$$= -\Delta A^{-1/2} \quad \text{for odd-odd nuclei.}$$

It may be noted here that correction terms such as the finite-size proton form factor term $[O(Z^2/A)]$ and the charge-anomaly Nolen-Schiffer term $[O(\beta A)]$ are found [14,18] to cancel exactly in the resulting INM equations, while other possible higher-order terms such as curvature and surface-symmetry are also seen [14,18] to be inconsequential in the INM model. Using the definitions for the Fermi energies noted above coupled with Eqs. (2.2)–(2.4), the HVH theorem [Eq. (2.1)] can be recast in terms of their counterparts for finite nuclei. The local energy $\eta$ being considered as the characteristic energy of a given nucleus is localized in nature

and conceptually treated on a different basis compared to the global terms. As a result of this ansatz, the sum of the terms in $\eta$ occurring on either side of the recast HVH theorem should be equal. The validity of this ansatz has been well demonstrated elsewhere [15,16] and hence needs no repetition here. This has resulted in decoupling the local energy terms from the global ones in the recast HVH theorem as

$$\frac{E^F(A,Z)}{A} = \frac{1}{2}[(1+\beta)\epsilon_n^F + (1-\beta)\epsilon_p^F] + S(A,Z) \quad (2.5)$$

and

$$\frac{\eta(A,Z)}{A} = \frac{1}{2}\left[(1+\beta)\left(\frac{\partial \eta}{\partial N}\right)_Z + (1-\beta)\left(\frac{\partial \eta}{\partial Z}\right)_N\right], \quad (2.6)$$

where

$$S(A,Z) = \frac{f}{A} - \frac{N}{A}\left(\frac{\partial f}{\partial N}\right)_Z - \frac{Z}{A}\left(\frac{\partial f}{\partial Z}\right)_N. \quad (2.7)$$

Furthermore, the infinite part $E[=E(A,Z)]$ must satisfy the generalized HVH theorem (2.1), whose solution is given by

$$E = -a_v^I A + a_\beta^I \beta^2 A. \quad (2.8)$$

A thorough analysis of the above equations followed by least-square fits in two steps (see Ref. [14] for details) leads to an accurate estimation of the model parameters, the values of which are

$$a_s^I = 19.271 \text{ MeV}, \quad a_c^I = 0.7593 \text{ MeV},$$

$$a_v^I = 16.108 \text{ MeV}, \quad a_\beta^I = 24.06 \text{ MeV}.$$

Further analysis [13] leads to determination of the pairing parameter $\Delta = 11.505$ MeV. Thus all the relevant global parameters required in the INM model are determined by fitting the model equations to the known masses of nuclei compiled by Audi and Wapstra [21].

Equation (2.2) can now be used as a mass formula provided $\eta$ is known. For this, we use the usual backward and forward definitions for the derivatives occurring in Eq. (2.6) to recast it as recursion relations of $\eta$'s of neighboring nuclei as

$$\eta(N,Z) = \frac{N}{A-1}\eta(N-1,Z) + \frac{Z}{A-1}\eta(N,Z-1),$$

$$\eta(N,Z) = \frac{N}{A+1}\eta(N+1,Z) + \frac{Z}{A+1}\eta(N,Z+1). \quad (2.9)$$

Using these relations the unknown value of $\eta$ of a given nucleus can be estimated from the neighboring ones if they are known.

## III. IMPROVED LOCAL-ENERGY NETWORK

The local energy $\eta$ plays a significant role as far as mass of a given nucleus is concerned. Therefore before one ex-
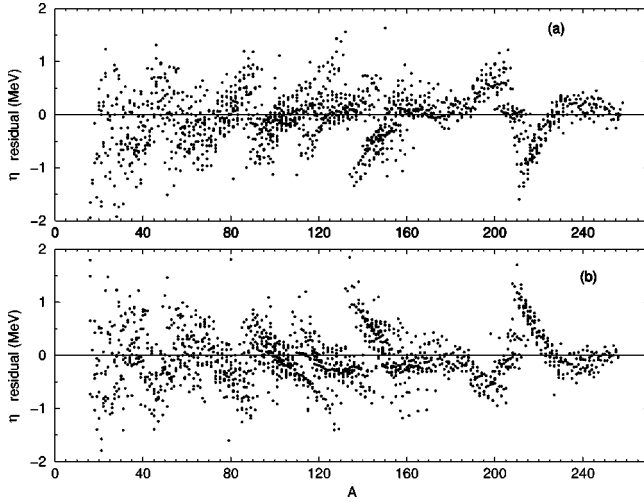
FIG. 1. The $\eta$ residuals of the recursion relations (2.9) calculated using the experimental local energies of all known nuclei for mass numbers $A$ beyond 15 as a function of $A$. The lower (a) and upper (b) regions, respectively, correspond to these two relations.



FIG. 2. Polygon showing the hierarchy of mesh points, each of which represents a nucleus having a given neutron and proton number connected to the four base nuclei represented by the line FG through the recursion relations (2.9).

ploits the relations (2.9) for this purpose, it is desirable to know to what extent these relations are satisfied with the known values. Accordingly, we use the values of the global parameters given in the previous section to calculate the experimental values of $\eta$ for all those nuclei whose masses are already known. These values can be further used to calculate the residual values of $\eta$ (also referred to as $\eta$ residuals), which are differences of the left- and right-hand sides of Eqs. (2.9) and are presented in Fig. 1 as a function of the mass number $A$. The appropriateness of these relations can be judged very well from the displayed residuals. The rms, as well as the mean deviation of these residuals, come out to be 0.528 MeV and 0.005 MeV, respectively, which clearly supports our contention about the validity of these relations. This not only reflects this contention but indirectly proves the appropriateness of our basic ansatz of the INM model, i.e., independence of the local energies from the global ones. In fact, the soundness of these relations had been amply demonstrated [15,16] in the past in constructing the first mass table based on these relations and thereby establishing the INM model as a mass formula.

However for the estimation of $\eta$ for nuclei far away from the known valley, our past method of extrapolation was found to be of limited applicability. This was due to an accumulation of errors in building up the values of $\eta$ very far from the known region. In fact, the old method was confined to a single least-square fit of the known nuclei lying in a polygon mesh (see Fig. 2), each mesh point of which corresponds to a given nucleus. As a result, depending on the actual site of a given nucleus with respect to the base nuclei (represented by FG in Fig. 2), the prediction error would go on increasing, thereby putting a kind of limitation on the past method. Apart from this problem, its estimation for the local energy of a given nucleus is also likely to vary, depending on the actual path chosen in the network, i.e., the choice of the base nuclei.

Hence to circumvent all these problems, we have recently
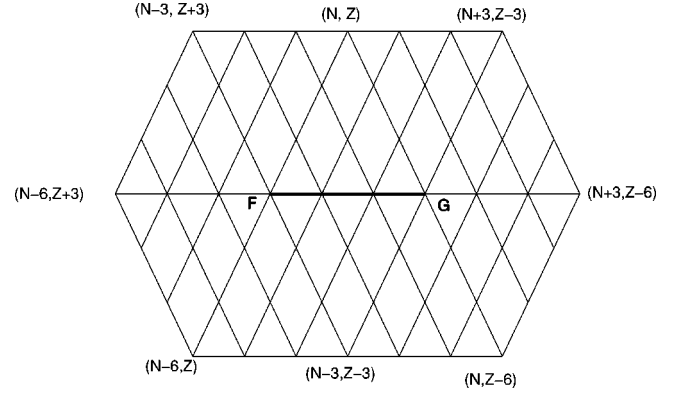
[13] devised a novel scheme to obtain the most expected value, following the ensemble-averaging of several alternative values $\eta_i$, which are generated by repeated application of the recursion relations (2.9) in all possible directions of the nuclear chart, starting from the known regions. In fact, a given mesh point representing a particular nucleus in the network is encountered several tens of times, as the local mesh in the form of the polygon (see Fig. 2) is made to roll both horizontally and vertically, each step of which corresponds to a least-square fit of the known data lying inside the polygon. This enables a given mesh point to be reached from all possible directions, both near as well as far from proximity of the data base. Effectively, the present method consists of repetition of the old method several times, each of which corresponds to different base nuclei. This results in generating an ensemble of values $\eta_i$ together with their associated errors $\sigma_i$ [22] for a given nucleus, which are then used to yield the expected value through the Gaussian-weighted averaging method:

$$\eta = \frac{\sum_i \eta_i \ \exp[-((\sigma_i - \sigma_0)/\sigma_{\text{rms}})^2]}{\sum_i \ \exp[-((\sigma_i - \sigma_0)/\sigma_{\text{rms}})^2]}, \qquad (3.1)$$

where $\sigma_0$ is the least of all the $\sigma_i$'s for a given nucleus and $\sigma_{\text{rms}}$ ($=401$ KeV) is the rms deviation of all the 1884 known-mass nuclei used in the fit. Interestingly the actual intermediate path connecting the given nucleus to the base nuclei (shown as FG in Fig. 2) is not relevant in this method, as the ensemble averaging procedure automatically takes care of all possible paths from the entire data base surrounding the nucleus, and is thereby expected to yield the correct value. Thus this method in a way provides a unique mechanism for calculating the correct values of the local energies for all nuclei throughout the nuclear chart, which is quite crucial for the success of the INM model as a mass formula.

Apart from this well-defined procedure for the estimation of $\eta$, we have introduced two constants $\delta_1$ and $\delta_2$ in the two recursion relations (2.9) with a view to achieve better agree-
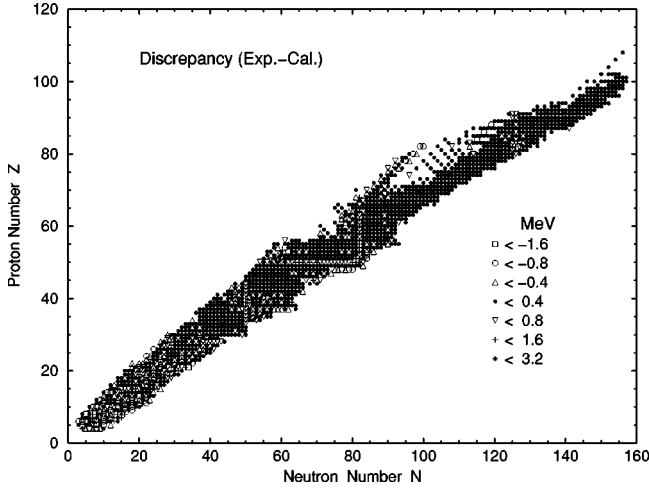
FIG. 3. Differences between the experimental (Ref. [21]) and calculated binding energies (BE) for the 1884 known nuclei.



FIG. 4. The $S_{2n}$ and $\eta$ isolines of some elements as a function of $N$, for several series of isotopes in the vicinity of the neutron magic number $N_m = 50$, 82, and 126, respectively. The solid or broken lines correspond to INM model values while open circles, triangles, etc., represent the experimental data points. All the conventional magic numbers are shown as vertical lines in the graph.

ment of those relations and thereby help us to predict the correct values. The values of these parameters are automatically determined each time, and the fitting procedure of the known local energies lying in the polygon is carried out. But these parameters simply act as internal intermediate aids of the calculation, as these are not relevant at the end of the calculation by virtue of the ensemble-averaging procedure of the generated values of $\eta$. In this sense the INM model is almost parameter-free, except of course for its having the five global parameters.

Following this procedure, we have generated the local energies and consequently the masses of about 7208 nuclei lying all over the chart confined to the ranges $4 \leqslant Z \leqslant 118$ and $8 \leqslant A \leqslant 270$, which includes nuclei up to and beyond the drip lines. Once the masses are known, it is just customary to calculate the derivative quantities like the two-neutron separation energies $S_{2n}$, which are used often in the present work. For sake of confidence in the model we present in Fig. 3 the binding energy residuals (difference between theory and experiment) as a two-dimensional plot, with neutron and proton numbers along the $x$ and $y$ axes, respectively. The various symbols show the magnitude of the residuals. From the nature of distribution of the residuals over the entire chart, one can judge very well the appropriateness of the model as well as the method of extraction of the local energies through the ensemble-averaging procedure.

## IV. CHARACTERISTICS OF THE MAGIC SHELL CLOSURES

In the present work, our main intention is to bring out the typical magic shell-closure behavior of the conventional magic nuclei and to analyze the same for those nuclides lying towards the drip regions of nuclear chart. Hence as a first step, we study these shell closures in the known $\beta$-stable regions, in which experimental results are very much available. Moreover, we are also interested in finding out any peculiar behavior of the local energies, which hitherto have been assumed to be associated with the characteristic local properties of nuclei. With this view we present in Fig. 4 the

calculated two-neutron separation energy $S_{2n}$ and the local energy $\eta$ isolines, which basically connect the corresponding values of the isotopes for a given element. We also present the experimental values wherever available for sake of comparison. We mention here that the $S_{2n}$ isolines are well-known [3,8,21] carriers of shell structure and more appropriately the shell closures. Moreover, these quantities are also considered to be sensitive enough to reflect [23] any onset of deformation. Hence in order to highlight the typical structures at the magic neutron number, we display the $S_{2n}$ isolines connecting the isotopes mostly in the vicinity of the magic neutron numbers 50, 82, and 126 as well as across the mid-shells for those elements in which the shell closure is conventionally considered maximum, i.e., $Z \simeq 40$, 50, and 82. As expected, the $S_{2n}$ isolines show sharp and typical jumps with characteristic bending both just above and below the usual magic neutron numbers. In fact, Borcea *et al.* [24] have also pointed out the existence of such sharp features in the experimental mass systematics. This typical bending in the $S_{2n}$ isolines at the magic neutron numbers is henceforth referred to as the *shell-closure bending*. Surprisingly, the local energy isolines (see Fig. 4) are also found to behave in a typical fashion, the structure of which is clearly Gaussian with peaks lying exactly at the same magic numbers. Moreover, compared to $S_{2n}$-typical jumps, the Gaussian structures in $\eta$ are rather prominently sharp, thereby providing a better yardstick for examining the shell-closure behavior. The width of these peaks can be seen to reflect the degree of magicity of the concerned magic numbers associated with the corresponding elements. For instance, for the magic neutron number $N_m = 50$, the magicity of Zr ($Z = 40$) shell closure is definitely more magic than that of Sr ($Z = 38$) and this is well reflected in the corresponding $\eta$ Gaussians. Similar behavior can also be seen at the other two magic numbers, 82 and 126. Hence such typical behavior in the local energy isolines at the magic neutron numbers in the form of sharp

Gaussians is henceforth referred to as the $\eta$ *Gaussian*.

It is further interesting to find the way the local energies change, with an increase or decrease of neutrons away from the concerned magic numbers. The $\eta$ distributions away from magic numbers on either side can be seen to be U shapes, the minima of which again correspond to the plateau region in $S_{2n}$ isolines. Incidentally these are well-known regions of highly deformed nuclei. Such typical structure of the $\eta$ isolines in the form of sharp Gaussians at the magic neutron numbers and flanked on either side by the U-shaped distributions for the isotopes lying in the mid-shells representing the well-deformed nuclei, and thus provide a distinguishable means of identifying the shell structure. The scenario in the $\eta$ isolines is quite interesting in the sense that both shell-closure behavior as well as extreme deformations are found to complement each other through well-defined structures. This is of course expected as both these features are like the two sides of a coin, and hence any physical quantity should more or less reflect this complementary behavior. Here in the $\eta$ isolines we find this distinguishing feature to be well reflected in the form of clear-cut structures. The values of $\eta$ for all other isotopes for a given element lying in between these two extremes i.e., the tip of the Gaussian and the adjacent minima of the U shape, would naturally correspond to an intermittent shell structure i.e., in between the maximum-deformed and perfectly magic closed-shell structure. Thus taking into account all of these features, the local energy $\eta$ can be very well inferred to manifest itself as the carrier of shell structure. This is a rather important result on the grounds that simply from the local energy systematics one could obtain qualitative understanding of the shell structure. It should be emphasized here, that nowhere in the model is any explicit knowledge of the magic numbers or the so-called shell corrections ever used, unlike the case with macroscopic-microscopic [10,11] ones for mass predictions. Here, in a more natural and transparent manner, the magic numbers as well as the accompanying shell-structure behavior unfold themselves purely from the typical systematics of the local energies. Thus, such behavior is indeed remarkable, because of the underlying implication for a qualitative understanding of the shell structure elsewhere in the nuclear chart.

In addition to unfolding the typical shell-structure behavior from Fig. 4, we can also observe the remarkable agreement of the model values with those of experiment. In fact, the quality of agreement with experiment is expected in view of the small rms deviation ($=401$ KeV) obtained [13] for masses of all those nuclei used in the calculation. In any case the degree of agreement clearly reflects the appropriateness of the model as well as the method of local energy extraction. This definitely builds confidence in the model for all predictive purposes.

## V. SHELL CLOSURES IN THE NEUTRON- AND PROTON-DRIP REGIONS

Having identified the typical shell-closure features in $S_{2n}$ and $\eta$, we are in a position to examine the same in the $n$- and $p$-drip regions. Therefore we present in Figs. 5–7 the rel-
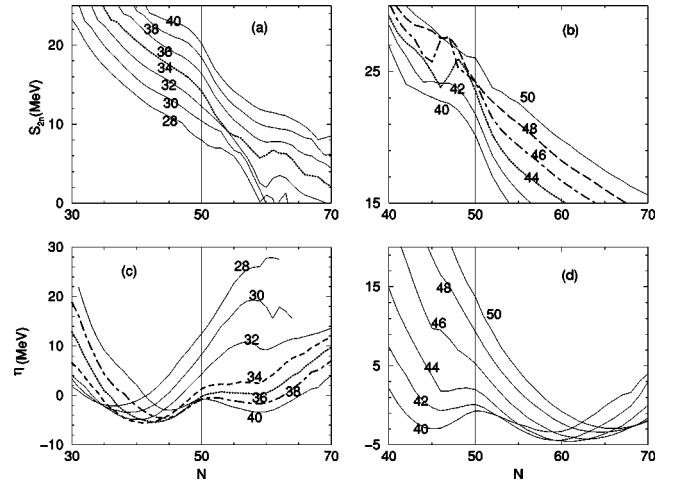


FIG. 5. The same as Fig. 3 indicating the gradual shrinking of the neutron magic shell $N_m = 50$ with varying proton number. Parts (a) and (b) display the $S_{2n}$ behavior in the neutron- and proton-drip region, respectively, while (c) and (d) represent similar aspects for the local energy $\eta$.

evant $S_{2n}$ and $\eta$ isolines of all the elements, progressively starting from the normal ones. In most of the figures, isolines of the neighboring even-$Z$ elements are displayed to note the varying changes in the typical shell-closure structure at the respective magic neutron numbers. Some of the neighboring isolines as well as the odd-$Z$ ones occurring very close to each other are not given to avoid clumsiness in the presentation. However those isolines not presented here are found to lie within the displayed ones at their appropriate places, and behave almost in a similar fashion. Hence in no way does their behavior influence the basic conclusions of the present work. Taking an overall view of the displayed $S_{2n}$ isolines in all the figures we find the typical *shell-closure bending* at the magic numbers gradually diminishes with a decrease or increase of proton number, which corresponds to an increase of neutron or proton excess, respectively. Ultimately in the extreme exotic neutron- or proton-rich regions, this bending almost vanishes implying strong quenching of
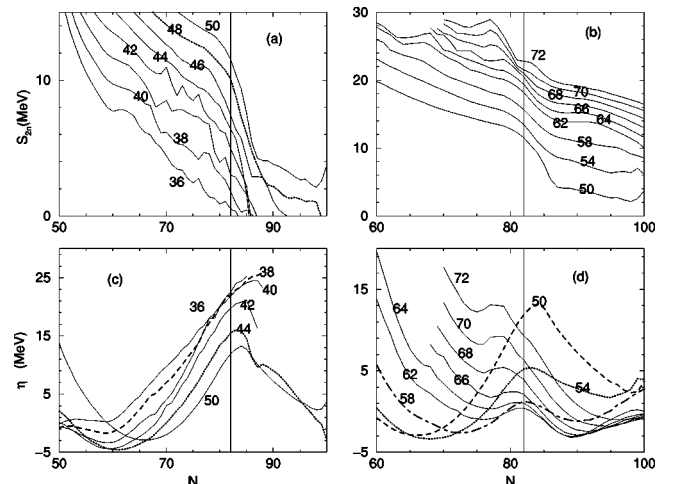


FIG. 6. The same as Fig. 4 corresponding to $N_m = 82$.
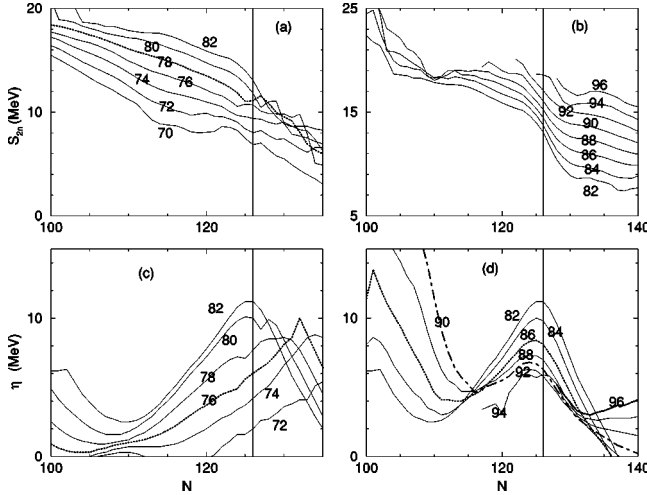
FIG. 7. The same as Fig. 4 corresponding to $N_m = 126$.

the magic shell closures at the conventional magic neutron numbers.

On the contrary, the behavior in the local energy isolines is quite interesting in the sense that they reflect the shell structure in a prominent and decisive manner, thereby implying strong repercussions on deformations as well as on magic shell closures. Again taking a bird's eye-view of the displayed $\eta$ isolines in Figs. 5–7, we find the $\eta$ Gaussians either shift to the neighboring neutron numbers or vanish beyond certain elements in both the $n$- and $p$-drip regions. It is further interesting to find this behavior accompanied by gradual vanishing of the typical U shapes in the $\eta$ isolines, either to the right or to the left of the magic neutron numbers, depending on the $n$-drip or $p$-drip region, respectively. Earlier we demonstrated that the U-shaped $\eta$ distributions representing the deformed regions and hence gradual vanishing of this structure clearly point to a decrease of deformations, finally implying no deformation at all in the event of their complete absence. In fact for such elements the U shapes in the corresponding isolines are replaced by monotonic variations. That means that all those nuclei lying in the drip-line regions and in the vicinity of the magic neutron numbers seem to have no deformation or magic closed-shell structure, which implies that these nuclei have some sort of *monotonous* or uniform shell structure. On the other hand, this also amounts to the disappearance of nuclear magicity, because magicity after all is a characteristic irregularity of the shell structure. This reduced deformability of those nuclei lying in the drip regions is an obvious consequence of the shell quenching of the concerned magic shells. Such a situation of reduced deformation in the drip regions is quite remarkable considering that a model study [9] involving ETFSI mass predictions having reduced deformations was found to remove the reported anomaly, earlier observed in the $r$-process nuclidic-abundance curves. Thus, such behavior in the shell structure in the exotic regions would definitely lead to vanishing of the shell gaps, which in fact is numerically shown later in this section.

Coming to the behavior of the magic number $N_m = 50$ in the neutron-rich region, we see from Fig. 5(c) that the $\eta$

Gaussians at $N = 50$ gradually diminish for the elements $Z$ as low as 34 and then ultimately vanish for the ones having the atomic number $Z < 34$. Naturally the corresponding U structures in the neighboring deformed valley (for $N > 50$) similarly vanish implying reduced deformability of those nuclei lying towards the $n$-drip line, and thereby amounts to increased shell quenching, thus tending to wash out the closed-shell structure. This behavior in $\eta$ is well supported by the $S_{2n}$ isolines [see Fig. 5(a)], in which case the typical *shell-closure bending* at $N = 50$ is almost absent for the same isolines ($Z < 34$). But unlike the local energies, the typical structure in $S_{2n}$ is not that remarkable, as noted earlier. However the monotonic variation for the elements $Z < 34$ is evident.

The behavior in the proton-rich region [see Fig. 5(b),(d)] is almost similar in nature. Here the U structure in the $\eta$ isolines in the lower $N$ side ($N < 50$) gradually vanishes for increasing values of proton number $Z$ and completely disappears beyond $Z = 44$. The gradual vanishing of the U structure is clearly seen to be synonymous with the diminishing behavior of $\eta$ Gaussians at $N = 50$. This clearly indicates the disappearance of neutron magicity of the magic number 50 with increasing proton excess. This behavior is well reflected in the $S_{2n}$ isolines [see Fig. 5(b)] as the corresponding ones ($Z > 46$) show monotonic variations around $N_m = 50$. An interesting feature can be noted in the behavior of $Z = 50$, as the $S_{2n}$ isoline shows a feeble jump at $N = 50$, while that of $\eta$ indicates a faint deviation, but devoid of any typical Gaussian structure. Such a feature may be attributed to a slight revival of nuclear magicity in this nucleus $^{100}$Sn, possibly arising due to the reinforcing action of the proton shell closure $Z = 50$, in spite of the fact that it is extremely proton-rich.

Similarly, the nature of isolines for both $S_{2n}$ and $\eta$ at $N_m = 82$ indicates disappearing magicity for $Z = 42$ downwards in the $n$-rich region [Figs. 6(a) and 6(c)] and beyond $Z = 66$ upwards in the $p$-rich region. The $S_{2n}$ isolines of these elements almost behave as monotonic variations around $N_m = 82$, while the $\eta$ Gaussian peaks of the corresponding $\eta$ isolines shift to the neighboring neutron numbers. But at these extreme neutron numbers the $n$-drip line is already reached for these elements ($Z < 44$), because values of both $S_n$ and $S_{2n}$ vanish. Hence the apparent shift of the neutron magic shell at $N = 82$ to the neighboring neutron numbers need not be taken seriously. Therefore all these aspects favor strong quenching of the neutron magic shell at 82 in this extreme neutron-rich region.

In contrast, the behavior of the $\eta$ Gaussians at $N_m = 82$ in the proton-rich region [see Fig. 6(d)] shows interesting variation, as the corresponding peaks gradually shift to the lower neutron side for the isolines beyond $Z = 66$. The same behavior can be viewed as gradual diminishing of the U structures indicating decreasing deformation in those nuclei lying in the regions $Z > 66$ and $N < 82$. From either point of view, it clearly amounts to the loss of magic closed-shell structure at $N = 82$ for the elements $Z > 66$. The $S_{2n}$ isolines of these elements shown in Fig. 6(b) can be seen to have reduced bending at $N = 82$, thus supporting the $\eta$ behavior on re-
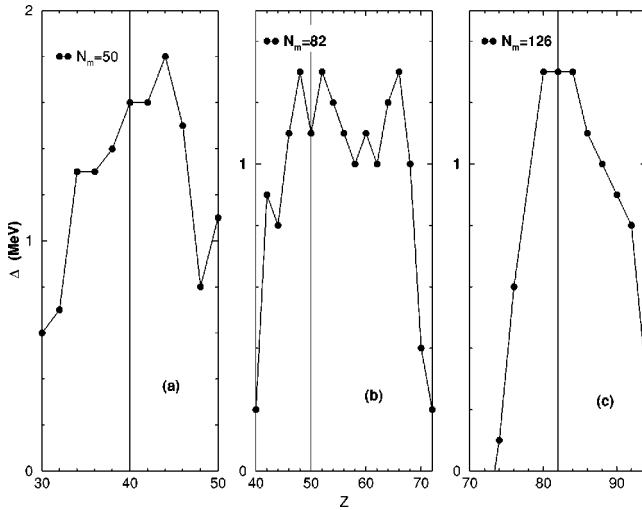
FIG. 8. The calculated shell gaps $\Delta(N_m)$ shown as dots and joined by a curve to guide the eye as a function of $Z$, for $N_m = 50$, 82, and 126. Those isotones conventionally expected to have maximum shell closure are indicated by vertical lines.

duced magicity. It is quite interesting to note that in the proton-rich region, the shell-closure behavior is well retained over a wide range of elements (almost from $Z=50$ to 64). This may be attributed to the reinforcing effect of the well-known [1] shell-closure behavior of the $Z=64$ shell, which again happens to be highly localized (see Ref. [1] for instance). This feature is very well reflected in the present study because with increase of proton numbers ($Z>64$), the magicity is drastically lost.

Concerning the behavior of magic number $N_m = 126$ in the neutron-rich region, the displayed isolines for $\eta$ in Fig. 7(c) clearly indicate shifting of the Gaussian peaks to the neighboring neutron number for the elements $Z$ less than 78. Similarly the corresponding $S_{2n}$ isolines also show monotonic variations instead of the shell-closure bending and thus support the $\eta$ behavior. Therefore such results very well imply the gradual shrinking of the magic shell closure at $N_m = 126$, followed by complete disappearance for those elements $Z$ less than 78. However in the proton-rich side, the $\eta$ Gaussians gradually diminish in height but never disappear and thus support the diminishing tendency of the magic shell closure at $N_m = 126$. However in this proton-rich region at such large values of $Z$, this model does not yield particle stable solutions for the isotones beyond $Z=94$. This is mostly due to the rapidly increasing Coulomb repulsion. The $S_{2n}$ isolines also can be seen to reflect this general behavior. The shell-gap calculation (see below) indicates the decreasing tendency of the shell gaps across the $N_m = 126$ shell with increasing proton excess. Thus from all these considerations one can say that there is a tendency of the 126 magic shell closure to gradually shrink. But with increasing proton excess around $Z=94$, the diminishing magicity cannot be discerned as clearly as the other two magic numbers discussed above.

In order to convey a quantitative idea for the degree of shell closure at the magic numbers, we present in Fig. 8, the calculated shell gaps defined by

$$\Delta(N_m) = S_n(N_m - 1) - S_n(N_m + 1), \qquad (5.1)$$

where $S_n$'s are the neutron separation energies. The $\Delta$'s clearly measure the change in the separation energy across the neutron-magic numbers and hence can be hailed as the measures of magic shell closure [6,8]. In fact the astrophysical $r$-process nuclidic abundance calculations [6] favor a gradual decrease of this gap towards $n$-drip line. From the displayed results presented in Fig. 8, one can clearly see that more or less these quantities vanish at all the magic numbers $N_m = 50$, 82, and 126, not only towards the neutron-drip line, but towards the proton-drip line as well. Hence these results suggest very well the gradual disappearance of neutron magicity of the concerned magic numbers, thus supporting all the features inferred from the systematic behavior of $S_{2n}$'s and $\eta$'s. There are however some fluctuations in the values of these gaps, such as for the isotones $Z=50$ and $N=82$ [see Fig. 8(b)], which may be attributed to the numerical inaccuracy of the calculated masses as they lie well within the rms deviation, which happens to be 0.401 MeV. Therefore for a qualitative understanding of the general behavior of the magic shell closures towards either of the drip lines, our calculated results on these shell gaps quite convincingly indicate the shell-quenching behavior of the neutron magic shells.

However, the systematic increase in these shell gaps towards the isotone $Z=66$ [see Fig. 8(b)] should not be taken as the result of numerical inaccuracy. It is rather due to the reinforcing action of the well-known localized shell closure [1] of the $Z=64$ shell as mentioned earlier. The observed drastic fall of the shell gaps for the elements beyond $Z=66$ is again a manifestation of the strongly localized nature of the $Z=64$ shell closure. It may be further noted that this quantity, which has been calculated from single-neutron separation energies, clearly supports all the features that we have inferred from the study of $S_{2n}$'s and local energies. This is an indication of the deep-rooted underlying behavior of the nuclear shell structure resulting in similar behavior on the part of physical quantities such as $S_n, S_{2n}$, etc.

Thus it is quite clear from all these considerations that in general the enhanced quenching of the neutron magic shells with increasing neutron (proton) excess is well established, the trend of which has been already seen from the known values in the low mass region [3,4]. We have also seen that this enhanced quenching towards the $n$- and $p$-drip lines is accompanied more or less by reduced deformability of those nuclei lying in the vicinity of the so-called neutron magic numbers, which possibly is the law of nature, because such reduced deformations in the exotic neutron-rich nuclei in a model study [9] involving the ETFSI model [10] were found to remove the reported anomaly observed in $r$-process nuclidic abundances. Incidentally in such extreme regions where deformations completely disappear, those nuclei would likely have *montonous* or uniform shell structure, which in bare terms means uniform single-particle levels near the Fermi level. This is only possible if the spin-orbit strength that causes the usual uneven shell structure vanishes towards the drip lines, which is in agreement with some of the recent calculations [25].

## VI. SUMMARY AND CONCLUSIONS

In summarizing the present paper we note that with a view to study the exotic behavior of magic shell closures in the extreme drip regions, we have to first establish the credentials of the INM model predictions in deriving the identifying typical structures associated with the so-called magic numbers in the known valley. With this approach, we have analyzed the two-neutron separation energies calculated from nuclear masses generated in the model, vis-a-vis the so-called local energies of the model, which in fact are the crucial quantities responsible for the success of the model as a mass formula. In this endeavor, we have succeeded in identifying the characteristic shell-closure features associated with the magic numbers 50, 82, and 126, both in case of two-neutron separation energies as well as the local energies. The shell-closure behavior in $S_{2n}$ isolines is well reflected by the typical bendings, termed the *shell-closure bending*. The local energies htat were hitherto assumed to be associated with the characteristic local properties of nuclei are invariably shown here to carry clear-cut signatures of the shell structure, through distinct structures in the form of sharp Gaussians at the usual magic numbers flanked on either side by the U-shaped distributions representing deformed nuclei. Thus, the $\eta$ isolines in the form of sharp Gaussians with the peaks lying exactly at the usual magic numbers, and flanked on either side by U-shaped distributions in the mid-shells representing the deformed regions, characteristically reflect the complementary nature of the underlying shell structure behavior. Therefore we conclude that the local energies can be considered as the carriers of nuclear shell structure.

In the second step, we have utilized these tools in examining the nature of the magic shell closures at $N_m = 50$, 82, and 126, for nuclei lying in the neutron- and proton-drip regions. Proceeding in a similar manner we found that, the typical *shell-closure bending* in $S_{2n}$ isolines gradually vanishes with an increase as well as decrease of the proton numbers relative to the normal $\beta$-stable ones. The $\eta$ distributions, which are expected to provide relatively sharp features, support very well the above behavior of the $S_{2n}$ isolines, as the corresponding $\eta$ Gaussians at the magic numbers are found to either vanish or shift to the neighboring neutron numbers. The U structure in the $\eta$ isolines corresponding to the deformed regions is found to progressively vanish initially, and vanish altogether beyond certain elements for those nuclei lying in the neutron- and proton-drip regions, thus implying reduced deformations in them. That means all these nuclei in the vicinity of the neutron magic numbers lying deep in the drip regions are neither deformed nor have closed-shell structure, which naturally implies some sort of monotonous or uniform shell structure near the Fermi level resulting in the disappearance of nuclear magicity. Interestingly, such a lack of deformation in the extreme $n$-drip region has been found to remove the reported anomalies in the $r$-process nuclidic abundances, as demonstrated [10] in a study involving the ETFSI model. On the other hand, the monotonous shell structure in the drip-line nuclei can be interpreted in terms of decreasing spin-orbit strength around the Fermi level. This follows from the fact that monotonous shell structure more or less means uniform distribution of single-particle levels near the Fermi level, which can be realized only if the spin-orbit strength vanishes towards the drip lines. This is in agreement with some of the recent calculations [25].

From these observations we finally conclude that the so-called *classical* magic numbers need not be universal and instead are localized in nature, as these are found to vanish with the increasing neutron or proton excess. More explicitly, the magicity of the magic numbers is found to depend on the relative composition of the concerned isotones.

Finally a word about the INM model itself is essential, without which our conclusions may be mistaken as model dependent. We would like to assert here that the basic conclusions on the shell-closure behavior are almost model independent, as nowhere in the model has either the concept of magic numbers or the so-called shell corrections been explicitly used. Rather, the distinguishing behavior of the characteristic local energies as well as the $S_{2n}$ isolines indicate the presence or absence of the magic shell closures. Moreover, the local energies which are the principal quantities singularly responsible for the success of the INM model as a mass formula are obtained through a well-defined ensemble-averaging procedure from a set of alternative values, generated by repeated application of the recursion relations from all possible directions of the nuclear chart. Consequently this method is most likely to yield the correct values of the local energies. Additionally our conclusions on the disappearance of nuclear magicity on the basis of the results of the INM model are well supported by the experimental trends in the low mass region, as well as in agreement with the implications of shell quenching as reported by the astrophysical $r$-process nuclidic abundance calculations.

[1] J. H. Hamilton, P. G. Hansen, and E. F. Zganjar, Rep. Prog. Phys. **48**, 631 (1985).

[2] K. L. Kratz, J. P. Bitouzet, F. K. Thielemann, P. Moeller, and B. Pfeiffer, Astrophys. J. **403**, 216 (1993).

[3] N. A. Orr *et al.*, Phys. Lett. B **258**, 29 (1991).

[4] O. Sorlin *et al.*, Phys. Rev. C **47**, 2941 (1993).

[5] F. K. Thielemann, K. L. Kratz, B. Pfeiffer, T. Rauscher, L. Van Wormer, and M. C. Weischer, Nucl. Phys. **A570**, 329c (1994).

[6] B. Chen, J. Dobaczewski, K.-L. Kratz, K. Langanke, B. Pfeiffer, F.-K. Thielemann, and P. Vogel, Phys. Lett. B **355**, 37 (1995).

[7] J. Dobaczewski, H. Flocard, and J. Treiner, Nucl. Phys. **A422**, 103 (1984).

[8] J. Dobaczewski, W. Nazarewicz, and T. R. Werner, Phys. Scr. **T56**, 72 (1995).

[9] J. M. Pearson, R. C. Nayak, and S. Goriely, Phys. Lett. B **387**, 455 (1996).

[10] Y. Abousier, J. M. Pearson, A. K. Dutta, and F. Tondeur, At. Data Nucl. Data Tables **61**, 127 (1995).

[11] P. Moeller, J. R. Nix, W. D. Myers, and W. J. Swiatecki, At. Data Nucl. Data Tables **59**, 185 (1995).

[12] S. Goriely and M. Arnould, Astron. Astrophys. **262**, 73 (1992).

[13] R. C. Nayak and L. Satpathy, At. Data Nucl. Data Tables (to be published).

[14] R. C. Nayak, V. S. Uma Maheswari, and L. Satpathy, Phys. Rev. C **52**, 711 (1995).

[15] L. Satpathy, J. Phys. G **13**, 761 (1987).

[16] L. Satpathy and R. C. Nayak, At. Data Nucl. Data Tables **39**,

213 (1988).

[17] J. M. Pearson, Phys. Lett. **91B**, 325 (1980); Nucl. Phys. **A376**, 501 (1982); F. Tondeur, J. M. Pearson, and M. Farine, *ibid.* **394**, 462 (1983).

[18] L. Satpathy, V. S. Uma Maheswari, and R.C. Nayak, Phys. Rep. (to be published).

[19] L. Satpathy and R. C. Nayak, Phys. Rev. Lett. **51**, 1243 (1983).

[20] N. H. Hugen Holtz and W. Van Hove, Physica (Amsterdam) **24**, 363 (1958).

[21] G. Audi and A. H. Wapstra, Nucl. Phys. **A565**, 66 (1993).

[22] B. R. Bevington, *Data Reduction and Error Analysis for the Physical Sciences* (McGraw-Hill, New York, 1969).

[23] X. Campi and M. Ephere, Phys. Rev. C **22**, 2605 (1980).

[24] C. Borcea, G. Audi, A. H. Wapstra, and P. Favron, Nucl. Phys. **A565**, 158 (1993).

[25] J. Dobaczewski, I. Hamamoto, W. Nazarewicz, and J. A. Sheikh, Phys. Rev. Lett. **72**, 981 (1994).